Journal of Applied Electrochemistry **30**: 1023–1031, 2000.

Simulation of influences of layer thicknesses in an alkaline fuel cell

J.-H. JO, S.-K. MOON and S.-C. YI
Department of Chemical Engineering, Hanyang University, Seoul 133-791, Korea

Received 18 January 2000; accepted in revised form 1 April 2000

Key words: alkaline fuel cell, mathematical modelling, simulation, single cell, thickness

Abstract

A computational simulation was conducted by using a one-dimensional isothermal model for an alkaline fuel cell (AFC) single cell to investigate influences of the thicknesses of the separator, catalyst layer, and gas-diffusion layer in an AFC. The cell polarizations were predicted at various thicknesses and their influences were also analysed. Thickening the separator layer decreased the limiting current density and increased the slope of the ohmic polarization region. Investigation on the thickness of the anode catalyst layer showed that the optimum thickness varied between 0.04–0.15 mm according to the cell voltage. The thickness of the cathode catalyst layer significantly influenced the cell performance. Also, a limitation of thickness effect in the cathode catalyst layer was observed. This limitation was considered to be caused by the mass transfer resistance of the electrolyte.

List of symbols

a^{g}	specific area of gas-electrolyte interface (cm^{-1})
a^{ℓ}	specific area of catalyst-electrolyte interface (cm^{-1})
C_i	concentration of species i (mol cm^{-3})
D_i	free stream diffusivity of species i (cm^2 s^{-1})
$\mathscr{D}_i$	effective diffusivity of species i (cm^2 s^{-1})
E	electrical potential of electrode (V)
E_{cell}	applied single cell voltage (V)
F	faradayic constant (96 485 C mol^{-1})
H_i	Henry's constant of species i (mol cm^{-3} atm^{-1})
I	current density of single cell (A cm^{-2})
I_L	limiting current density of single cell (A cm^{-2})
i	local current density (A cm^{-2})
i_o	exchange current density (A cm^{-2})
L	thickness of layer (cm)
N_i	molar flux of species i (mol cm^{-2} s^{-1})
n	number of electron transferred
P_i	partial pressure of species i (atm)
q_i	reaction order of species i
R	ideal gas constant (8.31451 J mol^{-1} K^{-1})
R_i^{e}	electrochemical reaction rate of species i (mol cm^{-3} s^{-1})
R_i^{p}	mass transfer rate of species i across phase boundary (mol cm^{-3} s^{-1})
R_{ohm}	slope of polarization curve in ohmic polarization region (Ω cm^2)
s_i	stoichiometric coefficient of species i
T	temperature (K)
t	time (s)
U	open-circuit potential (V vs NHE)
u_i	mobility of species i (mol cm^2 J^{-1} s^{-1})
$\mathscr{u}_i$	effective mobility of species i (mol cm^2 J^{-1} s^{-1})
v	volume average velocity (cm s^{-1})
y_i	vapour phase molar fraction of species i
z	spatial coordinate (cm)
z_i	charge number of species i

Greek symbols

α_a	apparent anodic transfer coefficient
α_c	apparent cathodic transfer coefficient
δ	thickness of electrolyte film (cm)
ϵ	porosity
ζ	dimensionless spatial coordinate
η	local overpotential (V)
κ	electrical conductivity (S cm^{-1})
κ_e	ionic conductivity of electrolyte (S cm^{-1})
σ	effective electrical conductivity (S cm^{-1})
τ	tortuosity
Φ	solution phase potential (V)

Superscripts

a	anode
c	cathode
g	gas phase
ℓ	liquid phase
e	electrochemical reaction
r	reference condition
p	mass transfer across a phase boundary
TF	PTFE
s	electrically conductive solid phase
θ	standard condition

Subscripts

a	anode
c	cathode
CL	catalyst layer
aCL	anode catalyst layer
cCL	cathode catalyst layer
e	electrolyte
GDL	gas-diffusion layer
aGDL	anode gas-diffusion layer
cGDL	cathode gas-diffusion layer
H	H_2
i	species *i*
j	species *j*
O	O_2
SEP	separator layer
w	H_2O
+	cation(K^+)
−	anion(OH^-)

1. Introduction

Thicknesses of separator, catalyst layer and gas-diffusion layer of fuel cells are known to affect cell performance. The performance of alkaline fuel cells (AFC) is also affected by these thicknesses. Although the effects of separator and gas-diffusion layer thicknesses are not known in detail, there have been many experimental or simulation investigations on the influences of the catalyst layer thickness in single electrodes for AFC [1–11]. Therefore, the influences of the catalyst layer thickness on the single electrode for AFC are relatively well known. However, by using only the results from the studies on single electrodes, it is difficult to correctly predict the performance variation of a single cell when the thickness is altered, because, within the single cell, the interactions between the layers are complicated, as shown by Kimble [12]. Furthermore, since the separator is commonly not taken into account in a single electrode model, it is almost impossible to predict its influence by using the single electrode model. A prediction using a single cell model can help to overcome such problems. Hence, development of a single cell model is necessary in order to study the effects of each layer thickness.

By using the simulation it is possible, not only to obtain the predicted cell polarization when a cell parameter is varied, but also to investigate the reason for the variation in the cell performance. Thus, a study on the effects of each layer thickness was conducted by using the one-dimensional single cell model developed in our previous work [13], where an 'orbiter fuel cell' of IFC (International Fuel Cell Corp.) was considered as a base-case model.

2. Description of system

The AFC single cell considered consisted of five layers: anode gas-diffusion layer, anode catalyst layer, separator layer, cathode catalyst layer and cathode gas-diffusion layer. A schematic diagram of the cell is shown in Figure 1. A detailed description of the model and basic phenomenon of an AFC is given elsewhere [13].

In the anode catalyst layer, dissolved hydrogen reacts electrochemically with hydroxide ions on anode catalyst surfaces, as follows:

$$H_2 + 2\,OH^- \rightarrow 2\,H_2O + 2\,e^- \tag{1}$$

The electron generated by the above reaction leaves the cell, then travels toward the cathode.

In the cathode catalyst layer, dissolved oxygen reacts electrochemically with water by the following reaction,

$$O_2 + 2\,H_2O + 4\,e^- \rightarrow 4\,OH^- \tag{2}$$

The hydroxide ion produced by the above reaction penetrates the separator, then reaches the anode catalyst layer.

From Equations 1 and 2 the overall reaction in an AFC is

$$H_2 + \frac{1}{2}O_2 \rightarrow H_2O \tag{3}$$

3. Mathematical modelling

Each layer of the cell was considered as a homogeneous continuum. This assumption is based on the macroscopic model presented by Newman and Tiedemann [14].

For a porous medium, the equation of continuity for species *i* can be written in general form as

$$\frac{\partial \epsilon C_i}{\partial t} = -\nabla \cdot N_i + R_i^{\mathrm{p}} + R_i^{\mathrm{e}} \tag{4}$$

where ϵ is porosity, t is time and C_i and N_i refer to the concentration and molar flux of species i, respectively.

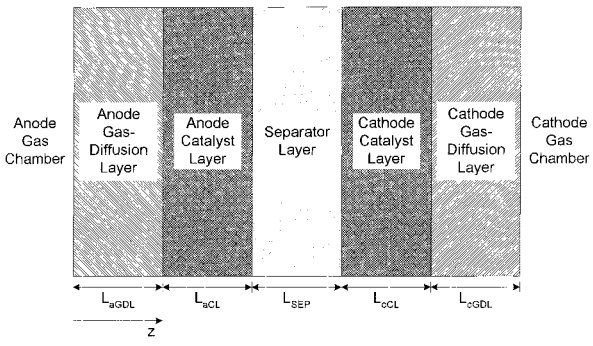

Fig. 1. Schematic diagram of an AFC single cell.

R_i^{p} and R_i^{e} indicate mass transfer rate across a phase boundary and electrochemical reaction rate of species i per unit volume of the electrode, respectively.

In the gas phase, the Stefan–Maxwell equation can be employed for N_i,

$$\nabla \cdot y_i = \sum_j \frac{RT}{P\mathscr{D}_{ij}^{\mathrm{g}}}(y_i N_j^{\mathrm{g}} - y_j N_i^{\mathrm{g}}) \tag{5}$$

where R is the gas constant, T is temperature and P is total pressure. The superscript 'g' indicates gas phase. y_i and $\mathscr{D}_{ij}^{\mathrm{g}}$ refer to gas phase mole fraction of species i and gas phase effective diffusivity of species i in j, respectively.

In the liquid phase, the Nernst–Planck equation can be employed for N_i:

$$N_i^{\ell} = -\mathscr{D}_i^{\ell}\nabla \cdot C_i - z_i \omega_i F C_i \nabla \cdot \Phi + C_i v \tag{6}$$

where F is Faraday's constant and Φ is the solution phase potential. $\mathscr{D}_i^{\ell}, z_i$ and ω_i indicate liquid phase effective diffusivity, charge number, and effective mobility of species i, respectively. The superscript ℓ in N_i^{ℓ} and $\mathscr{D}_i^{\ell}$ represents the liquid phase. The effective diffusivity, $\mathscr{D}_i$, is related with free stream diffusivity, $\mathscr{D}_i$, porosity, ϵ, and tortuosity, τ, as follows:

$$\mathscr{D}_i = \frac{\epsilon D_i}{\tau} \tag{7}$$

Similarly, the effective mobility, ω_i, can be expressed as

$$\omega_i = \frac{\epsilon^{\ell} u_i}{\tau^{\ell}} \tag{8}$$

If equilibrium is assumed at a gas–electrolyte interface, the mass transfer rate across the phase boundary, R_i^{p}, can be approximately described as

$$R_i^{\mathrm{p}} = -a^{\mathrm{g}} D_i^{\ell}\left(\frac{H_i P_i - C_i}{\delta}\right) \tag{9}$$

where a^{g} is specific area of gas–electrolyte interface, H_i is the Henry's law constant of species i and δ is the thickness of electrolyte film on catalyst surface. In the above equation, the minus sign in front of a^{g} indicates that species i goes out across a phase boundary. Hence, if species i come into current phase from the other, this sign will be changed to plus.

The electrochemical reaction rate per unit volume, R_i^{e}, can be represented as,

$$R_i^{\mathrm{e}} = -\frac{s_i a^{\ell} i}{nF} \tag{10}$$

where a^{ℓ} is the specific area of catalyst–electrolyte interface and n is the number of electrons transferred. The stoichiometric coefficient of species i, s_i, is given by expressing an electrochemical reaction in the form

$$\sum_i s_i M_i^{z_i} \rightarrow n\mathrm{e}^- \tag{11}$$

The local current density, i, is described by the Butler–Volmer equation,

$$i = i_{\mathrm{o}}\left[\prod_i \left(\frac{C_i}{C_i^{\mathrm{r}}}\right)^{q_i} \exp\left(\frac{\alpha_{\mathrm{a}} F\eta}{RT}\right) - \prod_j \left(\frac{C_j}{C_j^{\mathrm{r}}}\right)^{q_j} \exp\left(-\frac{\alpha_{\mathrm{c}} F\eta}{RT}\right)\right] \tag{12}$$

where i_{o} is exchange current density, C_i^{r} is concentration of species i at a reference condition, and q_i is reaction order of species i. α_{a} and α_{c} are apparent anodic and cathodic transfer coefficients, respectively. The local overpotential, η, is given by

$$\eta = E - \Phi - U \tag{13}$$

where E is the electrical potential at the electrically conductive solid phase U is theoretical open-circuit potential at a given concentrations and Φ is the solution phase potential. U is given by

$$U = U^{\theta} - \frac{RT}{nF}\sum_i s_i \ln\left(\frac{C_i}{C_i^{\theta}}\right) \tag{14}$$

where U^{θ} is the theoretical open-circuit potential evaluated at standard concentrations, C_i^{θ}, and temperature, T.

In a porous electrical conductive medium, the ohmic drop can be described by Ohm's law.

$$\nabla \cdot E = -\frac{1}{\sigma} \tag{15}$$

where I is total current density. The effective electrical conductivity, σ, is related to the bulk electrical conductivity, κ, volume fraction of electrically conductive solid phase, ϵ^{s}, and tortuosity of the phase, τ^{s} as follows:

$$\sigma = \frac{\epsilon^{\mathrm{s}}\kappa}{\tau^{\mathrm{s}}} \tag{16}$$

ϵ^{s} is associated with ϵ^{g}, ϵ^{ℓ}, and volume fraction of PTFE, ϵ^{TF}, as follows:

$$\epsilon^{\mathrm{g}} + \epsilon^{\ell} + \epsilon^{\mathrm{s}} + \epsilon^{\mathrm{TF}} = 1 \tag{17}$$

These general equations were employed to describe each layer. A more detailed description of the governing equations in each layer is given in previous work [13].

4. Model parameters

The entire base-case model parameters and correlations used in the present study can be found in our previous

work [13], and some of the parameters are listed in Table 1. The orbiter fuel cell, which is considered as the base-case model in the present study, is operated typically at 80 °C and 4.1 atm with 7 M KOH solution. Hence, these were considered as the base-case operating conditions for this work. During the variation of one parameter, another was fixed to the base-case value.

5. Method of solution

The model developed in our previous work consists of total 11 variables, 25 governing equations and 38 internal and outer boundary conditions. The governing equations and boundary conditions were discretized by using second-order and first-order finite difference schemes, respectively. The resulting finite difference approximations have a banded matrix structure, which can be solved by Newman's BAND algorithm [15].

6. Results and discussions

6.1. *Influence of separator layer thickness*

It is generally known that an increase in separator thickness L_{SEP} diminishes the cell performance, especially in the ohmic polarization region, thus the separator has to be as thin as possible. Figure 2, which shows an increase in the slope of the ohmic polarization region with increase in L_{SEP}, is consistent with such a fact. Simultaneously, it should be noted that Figure 2 represents a decreasing limiting current density I_L with increasing L_{SEP}. A similar result has been reported by Kimble and White [16]. It is accepted in general that I_L is not a function of separator properties as long as the rate-determining step is not in the separator. Since in the present model the rate-determining step at I_L exists in the cathode catalyst layer as shown previously [13], the decrease in I_L is difficult to understand. Thus we investigated whether the rate-determining step shifted from the cathode to the separator when L_{SEP} was varied. However, any evidence to prove the shift, for example, such as the existence of a region where electrolyte concentration C_e is very close to zero in the separator at I_L, was not found. Hence, the distribution of C_e through the cell was also investigated at I_L because a variation of C_e distribution can affect I_L. Note that the liquid phase diffusivities and solubilities of dissolved gases are functions of C_e.

Table 1. Some of the base-case parameters

Parameter (unit)	Gas-diffusion layers	Catalyst layers	Separator layer
L/cm	0.025	0.005 (anode) 0.010 (cathode)	0.005
ϵ^g	0.7	0.1	
ϵ^ℓ		0.6	0.8
ϵ^s	0.2	0.2	
τ	1.2	1.2	1.0
a^g/cm^{-1}		7.0×10^3	
a^ℓ/cm^{-1}		2.4×10^5	
δ/cm		5.0×10^{-5}	
i_o/A cm^{-2}		5.0×10^{-4} (anode) 5.0×10^{-8} (cathode)	

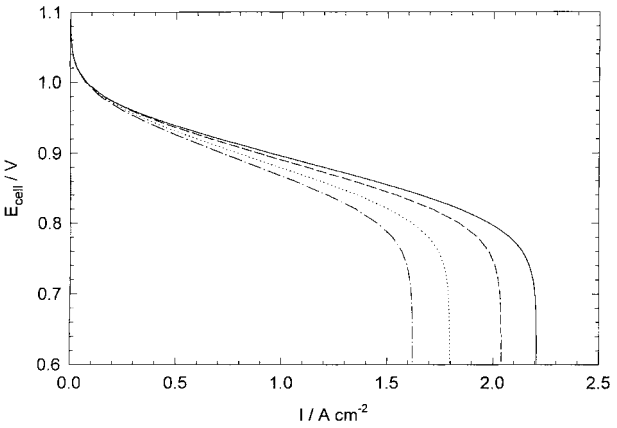

Fig. 2. Influence of separator thickness on polarization of AFC. L_{SEP}: (——) 0.05, (– – – –) 0.10, (· · · ·) 0.20 and (– · – · –) 0.30 mm.

Figure 3 illustrates the distribution of C_e at E_{cell} of 0.6 V which corresponds to I_L. Figure 3 also shows that C_e within the cathode catalyst layer increases with increasing L_{SEP}. It should be noted that an increase in C_e leads to a decrease in the liquid phase diffusivities and oxygen solubilities [17–19]. Hence, the decrease in I_L is considered to result from an increase in C_e within the cathode catalyst layer.

Figure 4 represents the slope of the ohmic polarization region R_{ohm} as a function of L_{SEP}. From this figure, it is confirmed that thickening of the separator increases R_{ohm} linearly. However, it is questionable whether the increase in R_{ohm} is due solely to an increase in ohmic drop within the separator layer, since a variation of I_L, as shown in Figure 2, can affect the value of R_{ohm} [20]. Hence, the ohmic drop within the separator layer $\Delta\Phi_{SEP}$ was investigated as a function of L_{SEP}, as shown in

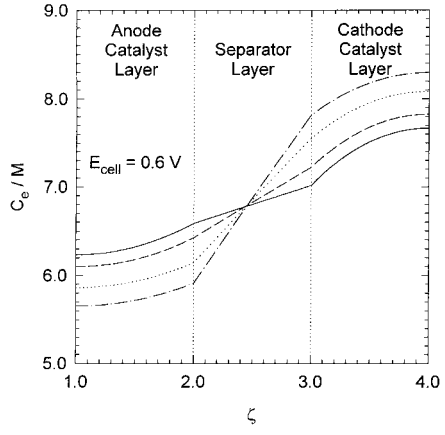

Fig. 3. Distribution of electrolyte concentration at several separator thicknesses. L_{SEP}: (——) 0.05, (– – – –) 0.10, (· · · ·) 0.20 and (– · – · –) 0.30 mm.

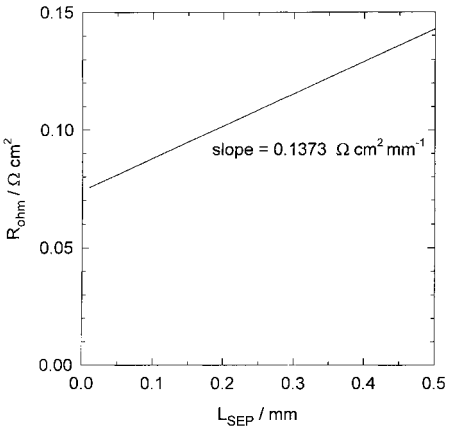

Fig. 4. Influence of separator thickness on slope of ohmic polarization region.

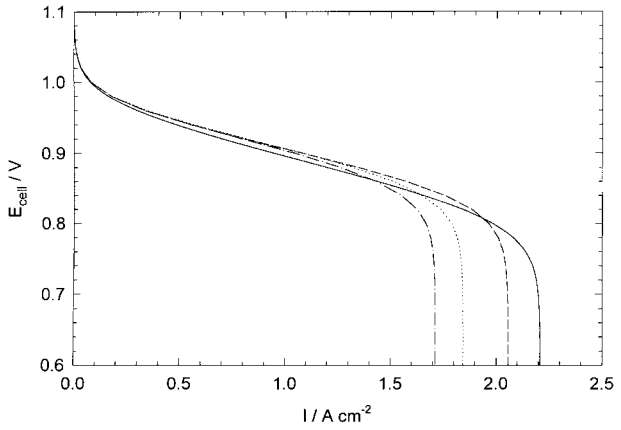

Fig. 6. Influence of thickness of anode catalyst layer on the polarization of AFC. L_{aCL}: (——) 0.05, (– – – –) 0.10, (· · · ·) 0.20 and (– · – · –) 0.30 mm.

Figure 5. A linear relationship between $\Delta\Phi_{SEP}$ and L_{SEP} was obtained, and the measured slope of the line was about 68.9 mV mm^{-1}. This value corresponds to 0.0689 Ω cm^2 mm^{-1} at 1.0 A cm^{-2}, while the slope in Figure 4 was about 0.1373 Ω cm^2 mm^{-1}. This suggests that 50.2% of the increase in R_{ohm} is attributable to the increase in $\Delta\Phi_{SEP}$. On the other hand, the remaining 49.8% is believed to be caused by the increase in mass transfer resistance of dissolved oxygen when the decrease in I_L, according to the increase in L_{SEP}, is taken into account.

6.2. *Influence of catalyst layer thickness*

The influence of the thickness of the catalyst layer, L_{CL}, is expected to be very significant, since the apparent reaction area and the apparent gas–electrolyte interface area of the catalyst layer are proportional to L_{CL}. In most cases, therefore, an increase in L_{CL} results in a linear increase in I, which is the 'thickness effect' [5], in all polarization regions. The increase in L_{CL} is expected particularly to cause a decrease in R_{ohm} and an increase in I_L. However, this expectation would be valid only for a single electrode, not for a single cell, since in a single cell complex interactions between layers may occur by thickening a catalyst layer.

6.2.1. *Anode catalyst layer*

Figure 6 illustrates the polarization curves as a function of the thickness of the anode catalyst layer L_{aCL}. When L_{aCL} is increased a decrease in I_L is observed with no large variation in the activation and ohmic polarization region. This result is considerably different from the expectation, since an increase in L_{aCL} is expected to enhance the cell performance. In particular, the decrease in I_L is not readily comprehensible, because the rate-determining step is in the cathode catalyst layer. However, like the case of the separator, if an increase in L_{aCL} causes an increase in C_e within the cathode catalyst layer, this tendency can be understood. Therefore, the C_e distribution at 0.6 V was investigated. Note that E_{cell} of 0.6 V corresponds to I_L as shown in Figure 6. In Figure 7, an increase in C_e in the cathode catalyst layer can be clearly seen as L_{aCL} increases. Thus the decrease in I_L is attributable to the increase in C_e in the cathode catalyst layer, which yields a decrease in the

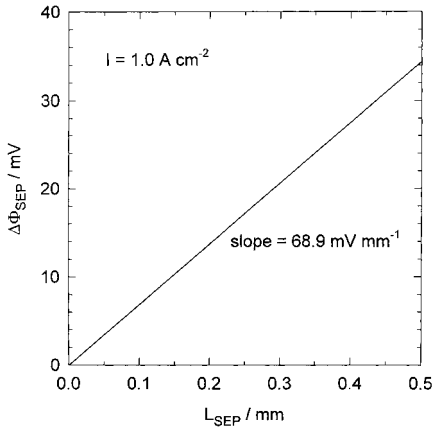

Fig. 5. Influence of separator thickness on ohmic drop in the separator.

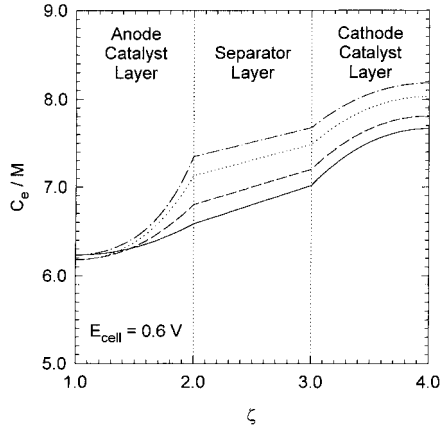

Fig. 7. Distribution of electrolyte concentration at several thicknesses of anode catalyst layer. L_{aCL}: (——) 0.05, (– – – –) 0.10, (· · · ·) 0.20 and (– · – · –) 0.30 mm.

solubility and liquid phase diffusivity of dissolved oxygen.

Figure 8 shows I as a function of L_{aCL} at various E_{cell}. I at 0.6 V, which is not shown in Figure 8, coincides with that at 0.7 V. As shown in Figure 8, the maximum in I is observed at L_{aCL} of about 0.15, 0.07 and 0.04 mm for E_{cell} of 0.9, 0.8 and 0.7 V, respectively, while the distinct maximum cannot be found at 1.0 V. In Figure 8, the decrease in I with increase in L_{aCL} on the right part of the maximum is thought to be caused by an increase in mass transfer resistance of dissolved oxygen when the decrease in I_L is taken into account. However, a dramatic decrease in I on the left part of the maximum can be seen with thinning of the anode catalyst layer. This seems to be caused by decreases in the apparent reaction and gas–electrolyte interface area of the anode catalyst layer due to the decrease in L_{aCL}. Especially, due to the extremely low apparent gas–electrolyte interface area of the anode catalyst layer on the left part, a shift in the rate-determining step at I_L from the cathode to the anode is expected. This is confirmed in Figure 9, which illustrates the distributions of dissolved gases at I_L when L_{aCL} is 0.02 mm. Unlike the case of the concentration of dissolved oxygen, C_O, the concentration of dissolved hydrogen C_H is seen to be close to zero. This suggests that the rate-determining step at I_L shifted from the cathode to the anode as expected. Therefore, if the case with 0.7 V in Figure 8 is taken into account, it is concluded that when L_{aCL} is smaller than about 0.04 mm the rate-determining step at I_L exists in the anode, not in the cathode. It is also considered that the decrease in I on the left part of the maximum in Figure 8 is caused mainly by an increase in the mass transfer resistance of dissolved hydrogen due to the extremely low apparent gas–electrolyte interface area of the anode catalyst layer.

6.2.2. *Cathode catalyst layer*

Because the activation and concentration polarization region are dominated by the cathode as confirmed in our previous study [13], altering the thickness of the cathode

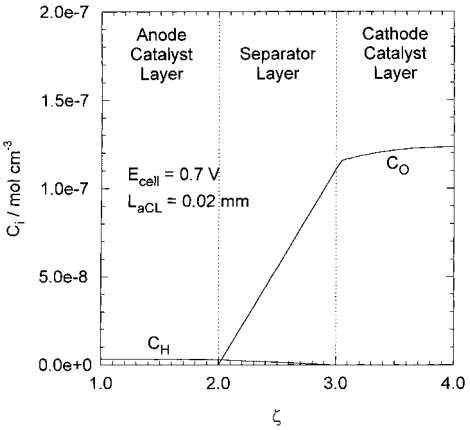

Fig. 9. Distribution of dissolved gases concentration at 0.7 V when thickness of anode catalyst layer is 0.02 mm.

catalyst layer L_{cCL} is expected to affect the cell performance considerably. Figure 10 indicates the validity of this expectation. Unlike the case of the anode catalyst layer, a large enhancement in the cell performance in all polarization regions with increase in L_{cCL} can be seen. This enhancement is made clearer by showing the power density of the cell. According to Figure 10, the power densities at 0.8 V are 0.93, 1.59, 2.35 and 2.83 W cm^{-2} at 0.05, 0.10, 0.20 and 0.30 mm in thickness, respectively. This suggests that the power density of about 3 W cm^{-2}, which is nearly two times larger than that of the base-case, can be obtained merely by increasing L_{cCL} to 0.30 mm.

Figure 11 illustrates the influence of L_{cCL} on I at various E_{cell}. Considerable increases in I as L_{cCL} increases are observed at most values of E_{cell}. In particular, the case with 1.0 V in Figure 11 shows a steady increase in I with thickening cathode catalyst layer. This indicates that the kinetic activity of the cathode is enhanced with increase in L_{cCL}. Note that the cathode dominates the activation polarization region of the polarization curve of the present single cell model, as mentioned above.

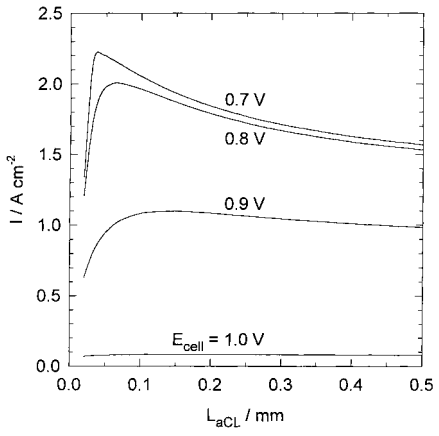

Fig. 8. Effect of thickness of anode catalyst layer on current density at various cell voltages.

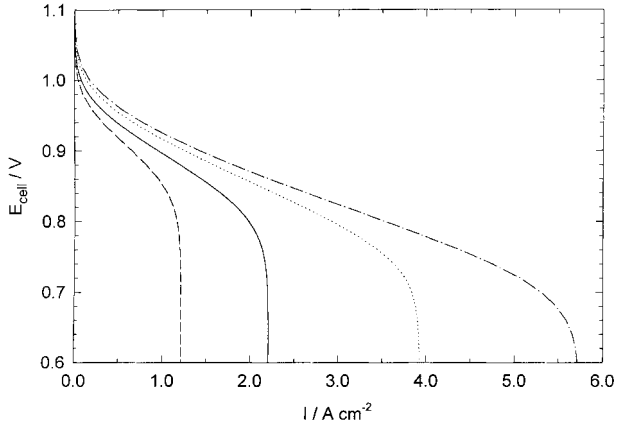

Fig. 10. Influence of thickness of cathode catalyst layer on polarization of AFC. L_{cCL}: (– – –) 0.05, (——) 0.10, (· · ·) 0.20 and (– · – · –) 0.30 mm.

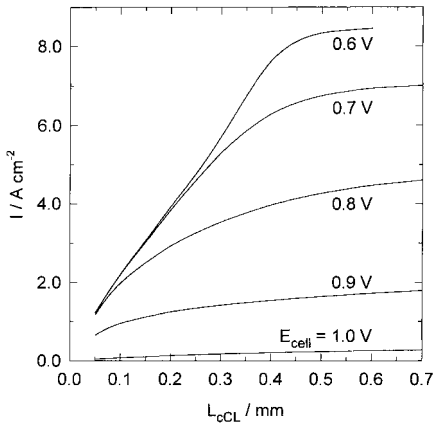

Fig. 11. Effect of thickness of cathode catalyst layer on current density at several cell voltages.

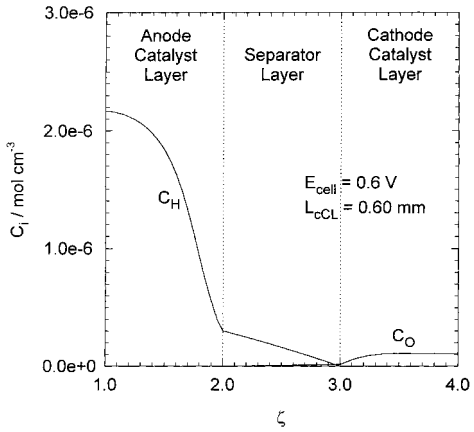

Fig. 12. Distributions of dissolved gases at 0.6 V, when thickness of cathode catalyst layer is 0.6 mm.

In the cases with 0.7 and 0.6 V in Figure 11, I increases almost linearly with thickness of the cathode catalyst layer up to ca. 0.45 mm, and reaches an upper limit beyond 0.45 mm. In spite of the differences in the operating condition and the electrode structure etc., a similar tendency was found elsewhere [3, 5, 9, 16]. In the literature, it has been reported that such phenomenon, the so called 'limitation of thickness effect', can be caused by gas phase diffusional resistance [9], diffusion [5] and migration [3] resistance of the electrolyte or high electrolyte concentration in the cathode [16], which causes a low solubility and liquid phase diffusivity of oxygen. Unfortunately, most of the studies mentioned above are for a single electrode except for that of Kimble and White [16]. By using numerical simulation, Kimble and White have already shown that the limitation of thickness effect can also occur in a single cell.

If interactions between the electrodes, as shown in the case of L_{aCL}, are taken into account, a possibility of a shift of the rate-determining step at I_L from the cathode to the anode could be considered as another reason for the limitation of thickness effect. It should be noted that a considerable decrease in the diffusional resistance of the dissolved oxygen due to an increase in L_{cCL} can lead to a shift in the rate-determining step toward the diffusion of dissolved hydrogen within the anode, since the diffusion resistance of the hydrogen is expected to be constant during the increase in L_{cCL}. If the liquid phase diffusion of the dissolved hydrogen becomes the rate-determining step, I_L will not vary with increase in L_{cCL}.

To identify the reason for the limitation of thickness effect in this cell, the shift in the rate-determining step, as mentioned above, was investigated preferentially. If the shift occurs at the upper limit of 0.6 or 0.7 V in Figure 11 as the cathode catalyst layer is thickened, C_H within the anode catalyst layer is expected to be close to zero. Figure 12 shows the distribution of C_H and C_O at the upper limit. As shown in Figure 12, unfortunately, C_H is much higher than C_O, which is not the expected result. This shows that the shift in the rate-determining step does not occur and the diffusion of dissolved oxygen is still the rate-determining step at the upper limit.

Secondly, the gas phase diffusion of oxygen was investigated under the same conditions to find whether this step is critical or not. However, the partial pressure drop of oxygen throughout the cathode catalyst layer is only ca. 0.229 atm as shown in Figure 13. Thus the gas phase diffusion does not seem to be the reason for the limitation of thickness effect either.

Diffusion of the electrolyte was also investigated. Figure 14 illustrates the distribution of C_e throughout the catalyst layers and the separator. As shown in the Figure the difference in C_e only within the cathode catalyst layer is nearly 5.8 M. This is a surprisingly large value. Hence, the diffusion of the electrolyte is considered as one of the reason for the limitation of thickness effect. It is also apparent that C_e within most regions of the cathode catalyst layer, except near the separator, is much higher than the initial electrolyte concentration, 7.0 M. For instance, C_e at the interface between the cathode catalyst layer and the cathode gas-diffusion layer is as much as about 9.2 M. Therefore, it is considered that decreases in the solubility and diffusivity of the dissolved oxygen due to the high C_e also occur

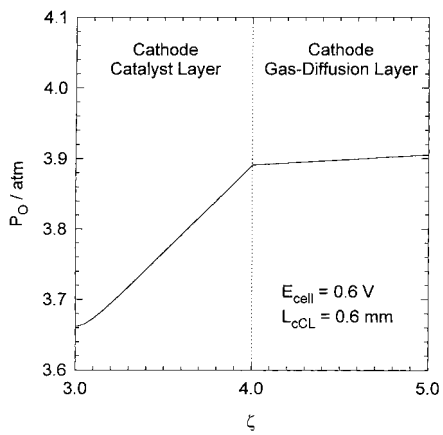

Fig. 13. Distribution of oxygen partial pressure in cathode at 0.6 V, when thickness of cathode catalyst layer is 0.6 mm.

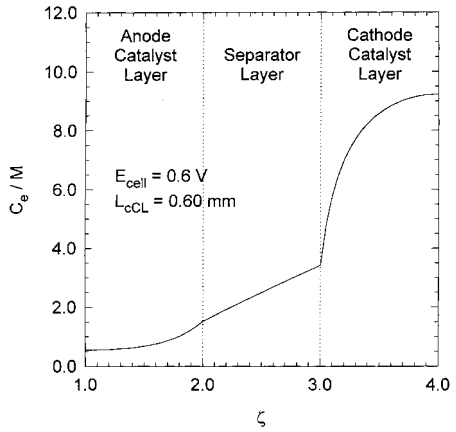

Fig. 14. Distribution of electrolyte concentration at 0.6 V, when thickness of cathode catalyst layer is 0.6 mm.

simultaneously, similar to the case of Kimble and White's study [16].

Additionally, the reason that the shift in the rate-determining step did not occur at the upper limit may be found in Figure 14. As shown, increasing L_{cCL} to 0.6 mm results in a considerable dilution of the electrolyte in the anode catalyst layer. This dilution implies an increase in the solubility and diffusivity of dissolved hydrogen within the layer, since a decrease in C_e increases the solubility and diffusivity of the hydrogen [17, 18]. That is, the diffusional resistance of the dissolved hydrogen within the anode decreases together with the decrease in diffusional resistance of the dissolved oxygen when L_{cCL} increases. Note that the shift in the rate-determining step from the cathode to the anode can occur when the diffusional resistance of the dissolved hydrogen is greater than that of the dissolved oxygen. It is, therefore, considered that the significant decrease in C_e within the anode, as shown in Figure 14, inhibits the shift in the rate-determining step.

Migration in the electrolyte was also investigated. As illustrated in Figure 15, the potential drop in the electrolyte within the cathode catalyst layer is as much

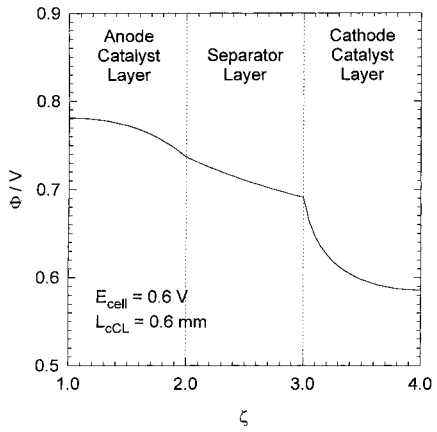

Fig. 15. Distribution of solution phase potential at 0.6 V, when thickness of cathode catalyst layer is 0.6 mm.

as 105 mV. This value corresponds to approximately one quarter of the total polarization. Hence, the migration resistance of the electrolyte is also thought to be significant.

Consequently, the mass transfer resistance of the electrolyte seems to lead to the limitation of thickness effect with respect to L_{cCL} in the AFC.

6.3. *Influence of gas-diffusion layer thickness*

Influences of the thicknesses of the anode and cathode gas-diffusion layer, L_{aGDL} and L_{cGDL}, respectively, were also investigated by varying the thickness from 0.05 to 0.55 mm. However, no noticeable variation in the polarization curve was found in this thickness range. This is considered to be attributable to the large diffusivities of gaseous hydrogen and oxygen. Thus, the gas phase resistances in both gas-diffusion layers are small. In AFC oxygen electrodes, there have been several reports that L_{cGDL} causes a significant variation in I_L [6, 9]. This is attributable to the possible non-uniform structure of the gas-diffusion layer, which can lead to a larger diffusional resistance of gaseous oxygen at the same porosity.

7. Conclusions

We investigated influences of the thicknesses of the separator, two catalyst layers and gas-diffusion layers on the performance of the AFC single cell by using a numerical simulation. Thickening the separator layer caused a decrease in the limiting current density and an increase in the slope of the ohmic polarization region. Decrease in the limiting current density was attributable to an increase in the electrolyte concentration within the cathode catalyst layer. It was also found that the increase in ohmic drop within the separator occupied nearly a half of the increase in slope of the ohmic polarization region when the separator thickness was increased.

Investigation of the thickness of the anode catalyst layer showed that there were optimum thicknesses in the range 0.04–0.15 mm, according to the cell voltage. Increasing the anode catalyst layer thickness resulted in a rise in electrolyte concentration in the cathode catalyst layer; thus the limiting current density was diminished. A shift in the rate-determining step at the limiting current density from the cathode to the anode was also found when the thickness of the anode catalyst layer was below 0.04 mm.

Thickness of the cathode catalyst layer influenced the cell performance significantly. Simultaneously, a limitation of thickness effect was also observed and considered to be caused by the mass transfer resistance of the electrolyte.

Although the influence of the gas-diffusion layer thickness was also investigated, no noticeable variation in the cell performance was found.

Acknowledgement

The authors thank CPRC (Ceramic Processing Research Center) of Hanyang University, Korea for partial support of this work.

References

1. J. Jansta and K. Micka, *Coll. Czech. Chem. Commun.* **35** (1970) 1650.
2. K. Mund and F.v. Sturm, *Electrochim. Acta* **20** (1975) 463.
3. K. Mund, G. Richter and F.v. Sturm, *J. Electrochem. Soc.* **124** (1977) 1.
4. T. Kenjo, *Bull. Chem. Soc. Jpn.* **54** (1981) 2553.
5. T. Kenjo, *J. Electrochem. Soc.* **132** (1985) 1583.
6. T. Kenjo and K. Kawatsu, *Electrochim. Acta* **30** (1985) 229.
7. T. Kenjo, *Denki Kagaku* **53** (1985) 957.
8. T. Kenjo and H. Shimizu, *Chem. Soc. Jpn.* **12** (1986) 1705.
9. P. Bjornbom, *Electrochim. Acta* **32** (1987) 115.
10. J.-H. Jo, H.-J. Kim and S.-K. Moon, *Hwahak Konghak* **34** (1996) 629.
11. J.-H. Jo, S.-C. Yi and S.-K. Moon, *Hwahak Konghak* **35** (1997) 838.
12. M.C. Kimble, PhD thesis, Texas A&M University, College Station, TX (1991).
13. J.-H. Jo and S.-C. Yi, *J. Power Sources* **84** (1999) 87.
14. J. Newman and W. Tiedemann, *AIChE J.* **21** (1975) 25.
15. J. Newman, *Ind. Eng. Chem. Fundam.* **7** (1968) 514.
16. M.C. Kimble and R.E. White, *J. Electrochem. Soc.* **139** (1992) 478.
17. S.K. Shoor, R.D. Walker, Jr. and K.E. Gubbins, *J. Phys. Chem.* **73** (1969) 312.
18. M.K. Tham, R.D. Walker and K.E. Gubbins, *J. Phys. Chem.* **74** (1970) 1747.
19. R.E. Davis, G.L. Horvath and C.W. Tobias, *Electrochim. Acta* **12** (1967) 287.
20. S. Srinivasan, D.J. Manko, H. Koch, M.A. Enayetullah and A.J. Appleby, *J. Power Sources* **29** (1993) 367.